Clim Dyn (2009) 32:615–634
DOI 10.1007/s00382-008-0440-4

A multi-model ensemble approach for assessment of climate change impact on surface winds in France

Julien Najac · Julien Boé · Laurent Terray

Received: 19 October 2007 / Accepted: 18 June 2008 / Published online: 14 August 2008

Abstract Statistical downscaling of 14 coupled atmosphere-ocean general circulation models (AOGCM) is presented to assess potential changes of the 10 m wind speeds in France. First, a statistical downscaling method is introduced to estimate daily mean 10 m wind speed at specific sites using general circulation model output. Daily 850 hPa wind field has been selected as the large scale circulation predictor. The method is based on a classification of the daily wind fields into a few synoptic weather types and multiple linear regressions. Years are divided into an extended winter season from October to March and an extended summer season from April to September, and the procedure is conducted separately for each season. ERA40 reanalysis and observed station data have been used to build and validate the downscaling algorithm over France for the period 1974–2002. The method is then applied to 14 AOGCMs of the coupled model intercomparison project phase 3 (CMIP3) multi-model dataset. Three time periods are focused on: a historical period (1971–2000) from the climate of the twentieth century experiment and two climate projection periods (2046–2065 and 2081–2100) from the IPCC SRES A1B experiment. Evolution of the 10 m wind speed in France and associated uncertainties are discussed. Significant changes are depicted, in particular a decrease of the wind speed in the Mediterranean area. Sources of those changes are investigated by quantifying the effects of changes in the weather type occurrences, and modifications of the distribution of the days within the weather types.

J. Najac (✉) · J. Boé · L. Terray
Climate Modeling and Global Change Team, CERFACS/CNRS, SUC URA1875, 42 Av. Gaspard Coriolis, 31057 Toulouse Cedex 1, France
e-mail: najac@cerfacs.fr

Keywords Statistical downscaling · Wind energy · Climate change · Multi-model ensemble · Impact study

1 Introduction

Near-surface winds have a strong influence on climate system and human activities. They play a major role at the air-sea interface affecting wave fields, surface fluxes and ocean mixing (Siegismund and Schrum 2001; Simmonds and Keay 2002; Fisher-Bruns et al. 2005; Wolf and Woolf 2006). As an example, the Mistral and Tramontana winds that originate in the Southeast of France and blow over the Gulf of Lion are key components of the Mediterranean Sea circulation (Millot 1999). Winds are also essential for building dimensioning, and may harshly affect crops (Cleugh et al. 1998): wind erosion, sandblasting, lodging, thigmomorphogenesis (modification of the plant growth due to the plant motion, mainly induced by the wind). Among climate community, wind speed extremes and gusts have received the most interest (Alexander and Tett 2005; Bärring and von Storch 2004). However, since wind energy is a fast growing renewable energy there is more and more interest in evaluating wind power potentials (Archer and Jacobson 2005), and in assessing any change in the wind distribution as a result of global warming (Bogardi and Matyasovszky 1996; Sailor et al. 2000; Pryor et al. 2005, 2006). This is particularly the case for France, as the Northwest and the Southeast of France are among the most attractive regions for wind energy in Europe (Troen and Petersen 1989).

The surface winds are mainly driven by the large scale circulation (LSC). However, several local features such as the surface roughness and the orography modify the spatial and temporal features of the surface winds. Because of

their coarse resolution, general circulation models (GCMs), cannot represent the small spatial scale variability of the near surface winds (Pryor et al. 2005). However, they show good skills in simulating the global climate and the LSC. To carry out an impact study we thus need to derive the high resolution climate state from the GCM's coarse resolution one (Giorgi and Mearns 1991). Different strategies have been developed to bridge this scale gap. They belong to the wide range class of the so-called downscaling techniques (Wilby et al. 2004). In the present study, we used a statistical downscaling (SD) technique.

The idea of the SD relies on the fact that the local climate is conditioned by two factors: the LSC and the local physiographic features such as the orography, the land cover, or the land-sea distribution. The observed relationships between the LSC and the local climate variables are used to set up a statistical model that enables to implicitly represent the interactions between the LSC and the local physiographic features (von Storch 1995). The main advantage of this method is that it is computationally little expensive. The main drawback of SD is the assumption that the empirical relationship between the predictors and the predictands remains stationary under future climate conditions. However, it is expected that the period over which the statistical model is implemented is long enough to contain a wide range of atmospheric situations. As a result, the statistical model should be able to handle successfully most of the future atmospheric situations provided that the large scale variables in the future climate lie roughly within the sampled variability of the present climate.

In the recent years, many SD studies have been carried out, mainly for surface temperature and precipitation. Concerning SD of surface wind speeds, only a few studies can be found in the literature. For instance, Pryor et al. (2005) uses the two parameter Weibull probability density function to represent the wind speed probability distribution (Hennessey 1977) at 46 stations in northern Europe. The downscaling methodology is then based on a multiple linear regression in which the monthly station-specific Weibull parameters are the predictands and the monthly means, and standard deviations of relative vorticity and mean sea level pressure gradients are the predictors. Sailor et al. (2000) develops a Neural Network transfer function to relate observed daily surface wind speed at three sites to a set of large scale atmospheric variables (wind speeds and geopotential heights at the surface, 850 and 700 hPa pressure levels, and sea level pressure). Kaas et al. (1996) carry out a canonical correlation analysis technique to reconstruct surface wind speeds at ten stations over the northern North Atlantic region using monthly means of sea level pressure and sea surface temperature fields as predictors.

As mentioned previously, one of the main advantages of the SD approaches is that the transfer functions that relate local variables to GCM large scale variables may be easily applied to several GCMs. This enables a multimodel approach that reinforces confidence in the results and provides an estimation of the uncertainty of the potential changes as the response of atmospheric circulation in climate change scenario simulations may be model dependent. Such multimodel studies were performed for wind speeds by Pryor et al. (2005, 2006) for northern Europe using respectively 5 and 10 GCMs. Pryor et al. (2006) showed that there was any consistent signal with regard to an increase or a decrease of the mean and 90th percentile wind speed or energy density over northern Europe in either climate projection period (2046–2065 and 2081–2100 for the IPCC SRES A2 experiment) relative to 1971–2000.

In the present study, we apply a SD method based on a weather regime classification that enables a day-to-day wind speed downscaling. We follow Boé et al. (2006) by first performing a classification of the observed days into a few groups (weather types) according to their synoptic similarity. Like other methods, this method provides several features that are of interest for our case of study. Firstly, it enables to identify dominant modes of circulation (Conil and Hall 2006). Secondly, the weather types enable to analyze the links between the LSC and the local climate on a physical point of view (Plaut and Simonnet 2001; Cassou et al. 2005). In particular, considering the LSC patterns only, the knowledge of the position of each day relative to the weather types may be sufficient to evaluate the associated local climate state (Gutiérrez et al. 2004). Thirdly, the weather type classification provides a powerful tool to cope with the multimodality of the distribution of some variables (for instance wind direction). Indeed, classification methods based on recurrence properties localize high concentrations of points in the classification space. Thus, the classification algorithm may allow to separate local maxima in the probability distribution function of the data in the classification space (Stephenson et al. 2004), and linear regressions may be applied within each weather type in order to recover the local climate state from the LSC. Last but not least, the weather type method enables to investigate sources of changes in the 10 m winds in the future in terms of large scale dynamical features. Indeed, the response of the climate system to external forcing may manifest itself in terms of excited modes of circulation (Corti et al. 1999; Stone et al. 2001). In that purpose, the weather types appear to be an interesting tool and partly justify our choice for this method.

The purpose of this paper is to present a SD method for surface winds and to carry out a multi-model ensemble study of the impact of climate change on surface winds in

France. In Sect. 2, the data and model used for the study are presented. Section 3 describes the SD methodology and Sect. 4 its validation. In Sect. 5 the SD is applied to different climate projections and differences with the current climate are discussed. Conclusions and perspective are presented in Sect. 6.

2 Data and model description

2.1 Near-surface wind speeds

Daily mean 10 m wind speeds and directions were extracted from the Météo-France (French meteorology service) SQR (Série Quotidienne de Référence) dataset (Moisselin et al. 2002). Daily mean wind speeds have been obtained by averaging 24 h values of wind speed measurements. We use wind speed and direction from this dataset at 78 stations over France for the period 1974–2002 (Fig. 1). The quality control of this dataset has been carried out by the Division de la Climatologie (DCLIM) service of Météo-France.

2.2 ERA40 Reanalysis

Zonal and meridian components of the daily mean 850 hPa wind over the period 1974–2002 were derived from the European Center for Medium-Range Weather Forecasts (ECMWF) ERA40 reanalysis (Uppala et al. 2005). 0000 UTC, 0600 UTC, 1200 UTC and 1800 UTC values at a 2.5° × 2.5° resolution were daily averaged. The predictor domain is represented in Fig. 1. A discussion of the choice of the predictor and the size of the predictor area is presented in Sect. 3.3.

2.3 Models

For the future climatic study, we use daily mean 850 hPa wind fields from 14 coupled atmosphere-ocean general circulation models (AOGCM) of the World Climate Research Program's (WCRP's) Coupled Model Intercomparison Project phase 3 (CMIP3) multi-model dataset, according to the daily data availability: BCCR-BCM2.0, CGCM3.1(T63), CNRM-CM3, CSIRO-Mk3.0, GFDL-CM2.0, GFDL-CM2.1, GISS-AOM, FGOALS-g1.0, INM-CM3.0, IPSL-CM4, MIROC3.2(medres), ECHO-G, ECHAM5/MPI-OM, MRI-CGCM2.3.2. Detailed documentation of the CMIP3 models can be found at http://www-pcmdi.llnl.gov/ipcc/model_documentation/ipcc_model_documentation.php. The horizontal resolution of these models varies between 1.875° × 1.875° and 4° × 5°. Daily mean 850 hPa wind fields have been interpolated onto the ERA40 2.5° × 2.5°grid. Three time periods are focused on: a historical period (1971–2000) from the climate of the twentieth century experiment and two climate projection

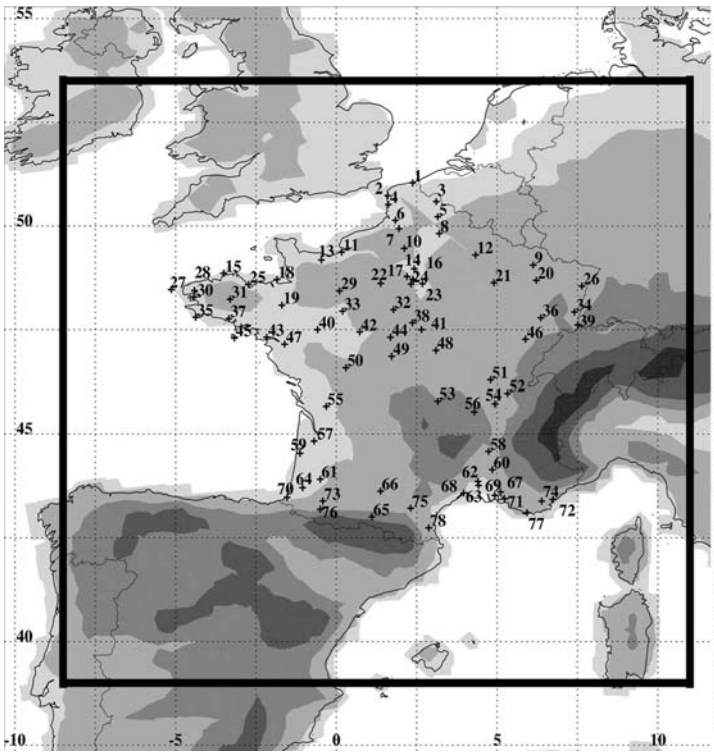

01 DUNKERQUE
02 BOULOGNE-SUR-MER
03 LESQUIN
04 LE TOUQUET-PLAGE
05 EPINOY
06 ABBEVILLE
07 DIEPPE
08 FONTAINE-LES-CLERCS
09 AUGNY
10 TILLE
11 SAINT-GATIEN-DES-BOIS
12 COURCY
13 CARPIQUET
14 BONNEUIL-EN-FRANCE
15 ILE-DE-BREHAT
16 VELIZY-VILLACOUBLAY
17 ATHIS-MONS
18 CANCALE
19 SAINT-JACQUES-DE-LA-LANDE
20 TOMBLAINE
21 SAINT-DIZIER
22 JALLANS
23 MONTEREAU-SUR-JARD
24 BRETIGNY-SUR-ORGE
25 PLEURTUIT
26 ENTZHEIM
27 OUESSANT
28 GUIPAVAS
29 ALENCON
30 LANVEOC
31 ROSTRENEN
32 BRICY
33 LE MANS
34 MEYENHEIM
35 PENMARCH
36 SAINT-SAUVEUR
37 QUEVEN
38 BOURGES
39 SAINT-LOUIS
40 AVRILLE
41 FARGES-EN-SEPTAINE
42 PARCAY-MESLAY
43 MONTOIR-DE-BRETAGNE
44 GIEVRES
45 BANGOR
46 OUGES
47 BOUGUENAIS
48 MARZY
49 DEOLS
50 BIARD
51 CHARNAY-LES-MACON
52 CHATEAU-GAILLARD
53 CLERMONT-FERRAND
54 BRON
55 CHATEAUBERNARD
56 ANDREZIEUX-BOUTHEON
57 MERIGNAC
58 MONTELIMAR
59 LA TESTE-DE-BUCH
60 ORANGE
61 MONT-DE-MARSAN
62 NIMES
63 SAINT-GILLES
64 DAX
65 LORP-SENTARAILLE
66 BLAGNAC
67 SALON-DE-PROVENCE
68 MAUGUIO
69 ISTRES
70 ANGLET
71 MARIGNANE
72 FREJUS
73 UZEIN
74 LE CANNET-DES-MAURES
75 CARCASSONNE
76 OSSUN
77 TOULON
78 PERPIGNAN

Fig. 1 850 hPa wind area is indicated by a *black square*, and stations providing daily mean 10 m winds by *numbers*. Six orographic levels are represented: 0, 100, 500, 1,000, 2,000, 3,000 meters

periods from the IPCC SRES A1B experiment: 2046–2065 (indicated by P1 in some figures) and 2081–2100 (indicated by P2 in some figures).

3 Methodology

The statistical downscaling method is an adaptation for this study of the method described by Boé et al. (2006). It has been implemented separately for two seasons: an extended winter season from October to March (6 months) called cold season and an extended summer season from April to September (6 months) called warm season (see Sect. 3.1 for a discussion of the definition of the seasons).

Thereafter, *UV*850 and *UV*10 refer to the 850 hPa and 10 m wind vectors (defined by both their zonal and meridional components), respectively.

3.1 Classification

The classification is achieved by implementing the widely used k-means algorithm (Michelangeli et al. 1995). The first step consists in performing a principal component analysis (PCA, based on the covariance matrix) to decrease the number of degrees of freedom of the system, as many of them represent just background noise that can be filtered out (Vautard 1990; Kaas et al. 1996; Plaut and Simonnet 2001). Combined empirical orthogonal functions (EOF) of the wind field component anomalies are computed (Kaihatu et al. 1998; Ludwig et al. 2004) (anomalies are calculated by removing the annual cycles). The first 10 and 12 EOFs of the *UV*850 and *UV*10 are retained to account for more than 80% of the total variance of both the *UV*850 and *UV*10. We then proceed as follows:

1. We classify the *UV*850 and *UV*10 together in the space spanned by the leading *UV*850 and *UV*10 EOFs. We get initial weather types defined by their centroids in the *UV*850 and *UV*10 EOFs state space.
2. The weather type centroids are determined in the space spanned by the *UV*850 EOFs only.
3. In the space spanned by the *UV*850 EOFs only, we assign each *UV*850 pattern to the closest centroid (reclassification), using the Euclidean distance as similarity measure: we get the final weather types defined by their centroids in the *UV*850 EOFs state space.

Thus, although the weather types are only defined by the LSC variables (the final weather types are only defined by the *UV*850), they remain discriminating for the 10 m wind (see Sect. 4.1) as the *UV*10 enter the preliminary classification (similar approach as Plaut et al. 2001; Boé et al. 2006).

Several statistical approaches to estimate the number of clusters to be retained in the classification can be found in the literature, most of them differing from each other by the measure of similarity. In the present study, the tests described by Michelangeli et al. (1995), Straus and Molteni (2004), and Levine and Domany (2001) have been computed. The Euclidean distance is used as the measure of similarity between points in the subspace of the retained EOFs. Only solutions that pass successfully through the three tests are kept. Accordingly, a six cluster partition is retained for both the cold and warm seasons.

The definition of the cold and warm seasons was actually achieved by first performing the weather type classification for the four classical seasons separately (December–January–February called DJF, March–April–May called MAM, June–July–August called JJA and September–October–November called SON). According to the statistical tests previously mentioned, we found the suitable number of clusters to be 6 for DJF, 5 for MAM, 6 for JJA, and 4 for SON. Then we performed a classification of the whole dataset using the 21 clusters previously calculated. We found that most of the days predominantly project onto either the JJA clusters or the DJF clusters, and that there was not any long and stable transition period between JJA and DJF and between DJF and JJA. We thus defined an extended summer season as the period over which the days predominantly project onto the JJA clusters (from April to September), and an extended winter season as the period over which the days predominantly project onto the DJF clusters (from October to March).

3.2 Regression

The final step consists in defining a way to relate the 10 m wind speed (*U*10) to the *UV*850 classification. Previous studies showed that the position of each day relative to the weather types could be a good predictor of the associated local climate state (Plaut et al. 2001; Gutiérrez et al. 2004). Thus, for each station and weather type, we have performed a multiple linear regression using the Euclidean distances between the *UV*850 weather type centroids and the *UV*850 patterns as the predictors and the observed 10 m wind speed as the predictand. Thus, for all days within a weather type we get a relationship of the form:

$$U10_i^{\mathrm{Reg}}(t_{p,k}) = \alpha_{p,i} + \sum_{j=1}^{N} \beta_{p,i}^{j}.d_{\mathrm{Eucli}}^{j}(t_{p,k})$$

where, $U10^{\mathrm{Reg}}$ is the 10 m wind speed reconstructed by regression, the subscript i refers to the ith station, $t_{p,k}$ is the kth day of the pth weather type, N is the number of clusters,

$\alpha_{p,i}$, and $(\beta^j_{p,i})_{1 \le j \le N}$ are the regression parameters for the station i and the weather type p, and d^j_{Eucli} is the Euclidean distance between the $UV850$ pattern of one day and the jth cluster centroid.

3.3 Final reconstruction

The variance of the 10 m wind speed downscaled in the way described previously is largely underestimated (underestimation of −35% for the cold season and −25% for the warm season, on average over all stations). Indeed, as the predictor does not completely specify the predictand, the whole predictand variability cannot be fully reproduced (von Storch 1999). Therefore, we add a final step based on an analog method in order to empirically increase the variance (similar approach as Boé et al. 2006).

The method can be divided into three steps summarized in Fig. 2. Let us consider a given day t_i for which we seek to estimate the 10 m wind speed and for which we only know the 850 hPa wind ($UV850(t_i)$).

1. The N Euclidean distances between $UV850(t_i)$ and the N weather type centroids are first computed in the $UV850$ EOF space. We identify the closest weather type WT^p by determining the minimum of these distances.
2. Secondly, the 10 m wind speed of this day is reconstructed using the WT^p regression coefficients, thereafter referred to as $U10^{Reg}(t_i)$.
3. Thirdly, spatial root-mean-square differences (RMSE) are computed between $U10^{Reg}(t_i)$ and all the reconstructed value $U10^{Reg}$ of the days belonging to WT^p in the learning period. We select the day t_m for which the RMSE value is minimal. Finally, we consider the corresponding observed 10 m wind speeds for this day t_m as our best estimate for the final downscaled wind speed $U10^{Down}(t_i)$.

If day t_i belongs to the learning period and observed or reanalyzed predictors are used (for example, present climate reconstruction with ERA40 predictors for the cross-validation procedure), the neighbor days of day t_i are excluded from the learning period. The neighbor days are defined as the days that belong to the same year. For example, if we reconstruct the 10 m wind speed for the first of February of 1982 with ERA40 predictors, the learning period will consist of all cold seasons except the 1981/1982 one. In Sect. 4.2, we apply this method when performing a cross-validation of the downscaling algorithm. Therefore, as the atmospheric synoptic time scale is about one or two weeks, we account for persistence properties that could produce

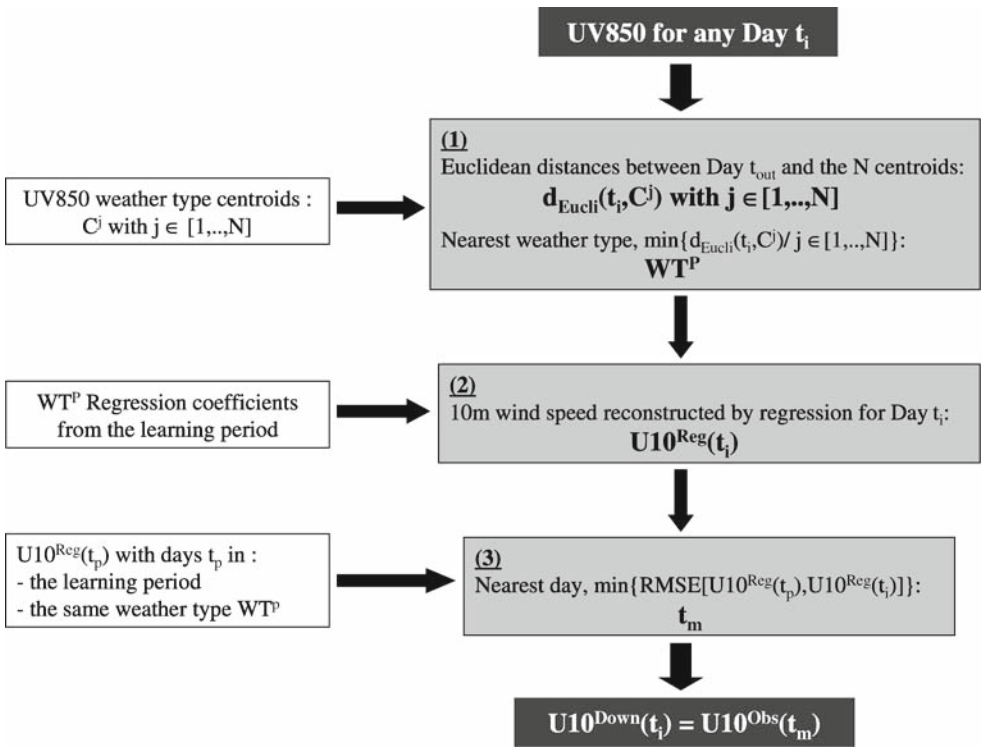

Fig. 2 Successive steps of the statistical downscaling method for 10 m wind speeds. $UV850$ stands for the zonal and meridional 850 hPa wind anomaly components. N stands for the number of weather types. $U10^{Down}$ stands for the downscaled 10 m wind speed. $U10^{Obs}$ stands for the observed 10 m wind speed. RMSE stands for the root-mean-square difference

artificial skills, and we can consider the downscaled days to be independent of the learning period.

One may wonder about the relevance of the regression step. For instance, we could skip the regression step and simply select a day according to minimum distances to the weather type centroids. However, the regression step enables to significantly improve the final results (for instance RMSE is reduced by 6% on average) as observed linear statistical relationships between *UV*850 and *U*10 are thus implemented in the algorithm.

Similarly, the condition of the search of an analog within the same weather type may seem superfluous as we would expect the analog day to systematically belong to the same weather type. This is actually the case for about 92% of the days. As a result this condition is meaningful for about 8% of the days.

As a part of the validation procedure, this method has been confronted to other downscaling methods (see Sect. 4.2). Focusing on some classical diagnoses, we show that our method provides good overall performances compared to the others, even if differences are sometimes small and that the performances of each method differ according to the diagnoses. However, beyond the more or less good performance of our method with regard to others, its main justification remains the opportunity to provide physical interpretations of changes in the surface winds thanks to the weather types.

The performance of the method has been also evaluated using different predictors: sea level pressure (SLP), 500 hPa geopotential height (Z500), 500 hPa relative vorticity (Vo500). All these variables have strong dynamical links with the 10 m winds. We found that the *UV*850 outperformed the other predictors. Furthermore, combinations of different predictors did not improve the results significantly or remained outperformed by the *UV*850 alone.

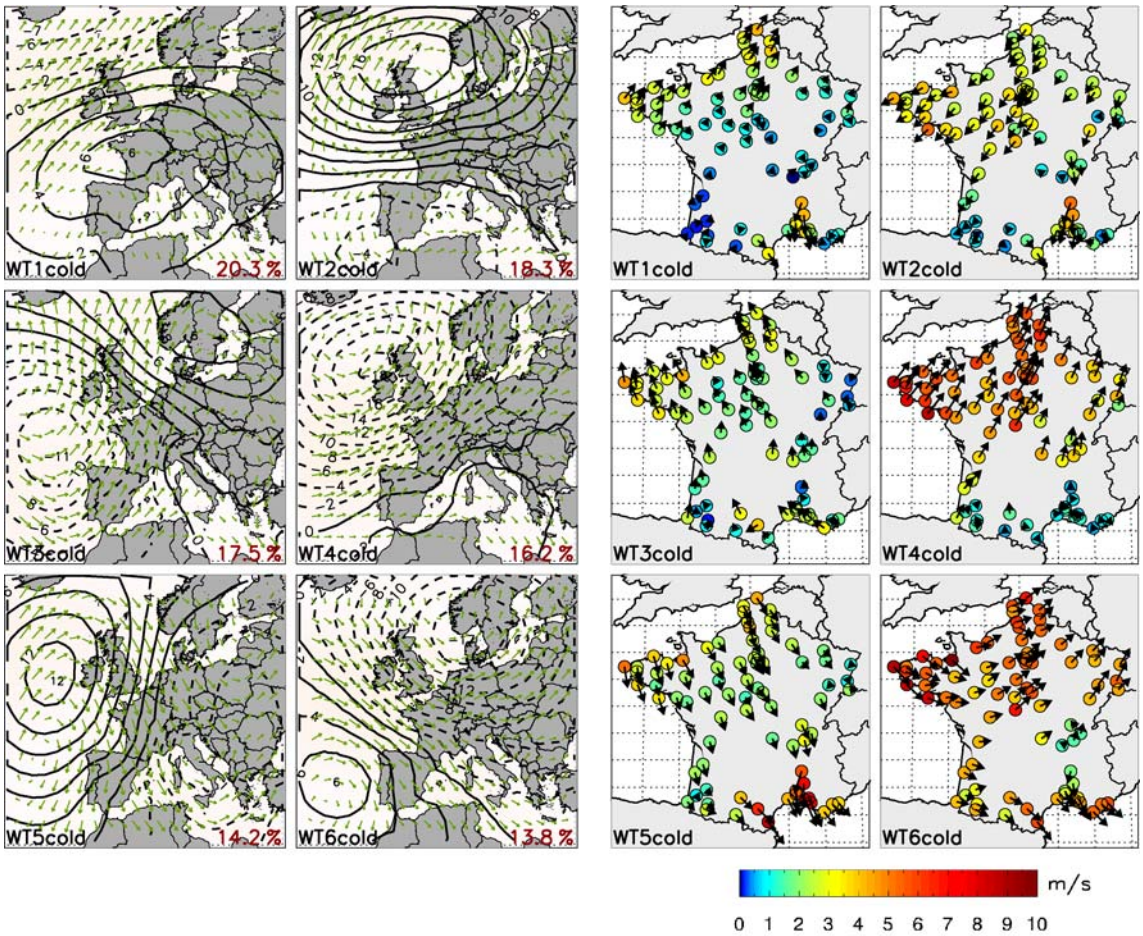

Fig. 3 SLP anomaly (contours every 2 hPa) and 850 hPa wind (*arrows*) composites (*left panel*), and 10 m wind composites (m/s) (*right panel*) for the weather types of the cold season (1974–2002). *Left panel*: *arrows* indicate wind directions, arrow length is proportional to wind module (varying between 0 and 18 m/s). *Right panel*: *color shading* represents wind module and *arrows* indicate wind directions (arrow length is proportional to wind module). Weather type occurrence (%) is indicated in the bottom left-hand corner of each panel. Composites are defined as the average fields of all days that belong to the same weather type

Moreover, different predictor domains have been tested, from a small domain centered over France to a large North Atlantic domain. On the one hand, the performance of the method (RMSE, daily correlation) was found to decrease when the size of the domain increases. On the other hand, the ability of the CMIP3 models to represent the large scale circulation at the synoptic scale (estimated by means of Taylor diagrams—see Sect. 5.2.1) was found to decline when the size of the domain decreases. The domain which has been selected appeared to be a good compromise.

4 Validation

4.1 Weather types

Figure 3 shows the average 10 m wind for each weather type of the cold season and the corresponding average sea level pressure (SLP) anomalies and average 850 hPa wind. All the weather types represent classical synoptic situations which are well known by meteorologists (personal communication from forecasters at Météo-France, Jiang et al. 2003 for some of the weather types). As an example, $WT5_{cold}$ is characterized by a SLP positive anomaly over the Atlantic Ocean and a negative anomaly over Eastern Europe. This synoptic situation is associated with northerly winds all over France, the geostrophic flow being highly accelerated near the Mediterranean Sea by the mountains (Pyrenees, Massif Central, Alps). This generates the well known Mistral which blows from the North in the valley between the Massif Central and the Alps, and the Tramontana which blows from the Northwest in the valley between the Pyrenees and the Massif Central.

Weather types for the warm season have slightly different patterns with weaker anomaly intensities (Fig. 4). They also represent well known synoptic situations.

In order to assess the relevance of the weather type classification, several diagnoses concerning its discriminating skills have been performed. As expected, the 10 m wind variability is significantly weaker within the weather types than when considering the whole dataset. This is highlighted by Fig. 5, for two stations which exhibit different surface wind features and are good representatives of two regions of interest for wind energy, namely Station 27

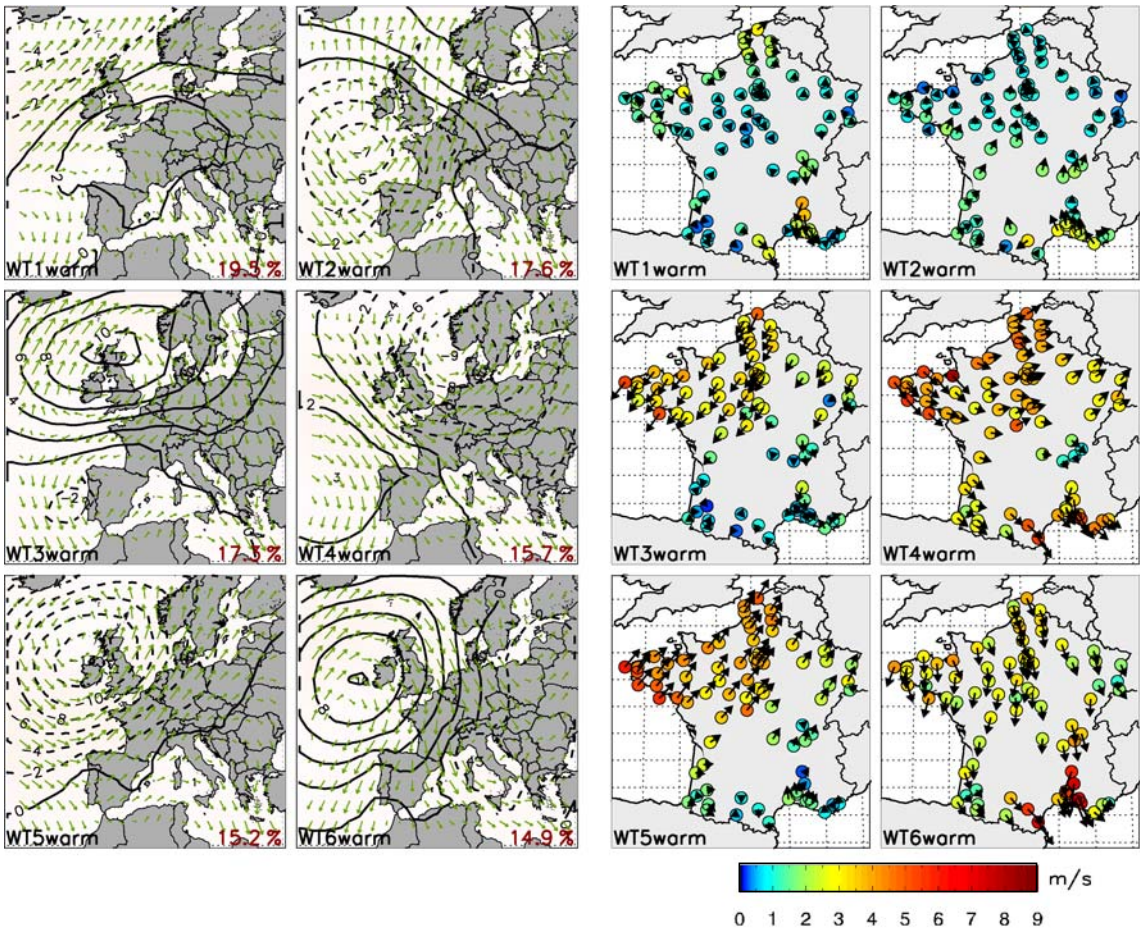

Fig. 4 Same as Fig. 3 but for the warm season

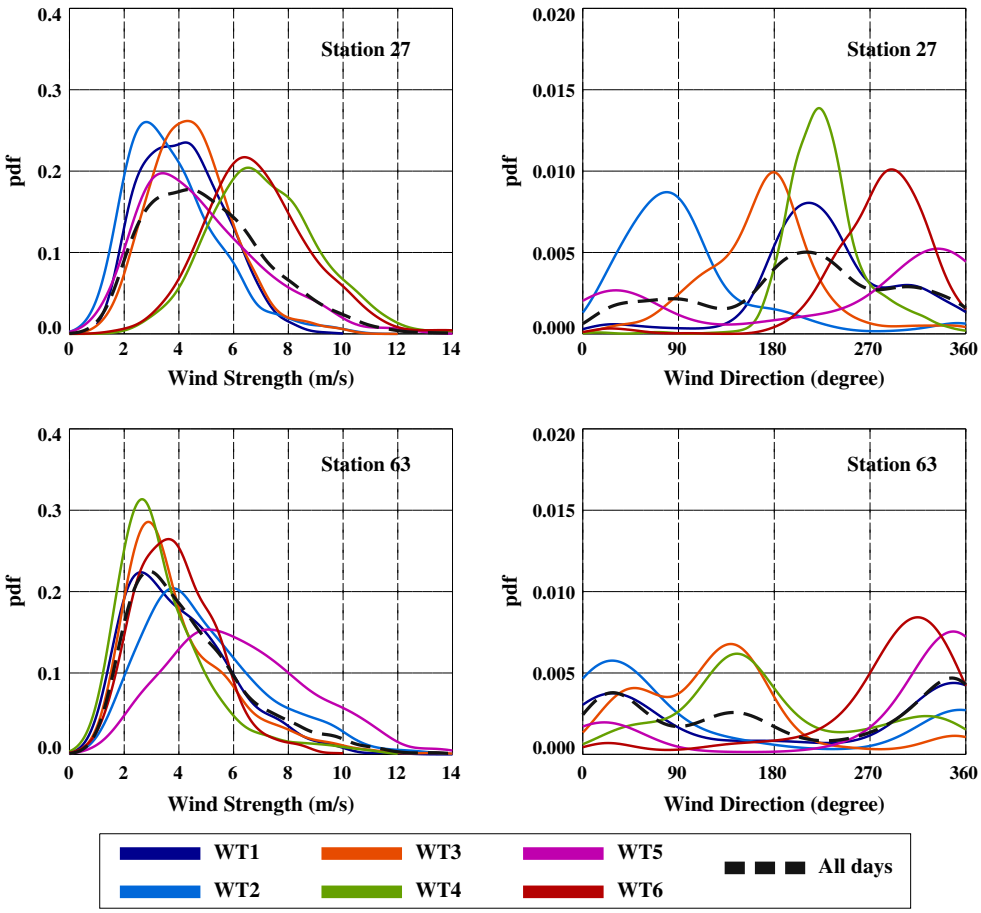

Fig. 5 10 m wind speed (m/s) (*left panels*) and direction (*degree*) (*right panels*) distributions within each weather type (*colored* lines) and for the whole dataset (*dashed black* line), for the cold season (1974–2002) at Station 27 on the upper panels and at Station 63 on the lower panels

in northwestern France and Station 63 in southeastern France. As is shown by this figure, the weather type classification enables to aggregate days with similar surface wind properties. Indeed, the spread of the probability density functions (pdf) is generally much smaller within the weather types than when considering the whole dataset. This confirms that the classification algorithm enables to minimize the variance within clusters with regard to the 10 m winds. Furthermore, while the 10 m wind direction pdf is multimodal when considering the whole dataset, the pdf within the weather types tend to be having unimodal shapes. The means of both 10 m wind direction and speed within the weather types are also clearly different, which suggests that the weather types are well separated and capture distinct atmospheric situations with respect to the 10 m winds.

4.2 Downscaling validation

As only one short complete observed 10 m wind speed dataset was available (from 1974 to 2002), it has not been possible to validate the downscaling algorithm over an independent time period. As a consequence, the method has been cross-validated over the whole learning period (1974–2002) (see Sect. 3.3 for definition of the cross-validation).

While the downscaling algorithm is applied separately for each season, the performance of the method is similar for both seasons. As a result, we only show results for the two seasons together in the following.

Daily linear correlation, RMSE, mean error, standard deviation error, 90th and 10th percentiles (P90, P10) errors are shown in Fig. 6 for each station (in this study, all daily linear correlations have been computed on time series in which the annual cycle has been filtered out). First of all, it can be seen that results from the downscaling match well with the observations (high correlation coefficients and weak errors in most stations), and that there is not any clear recurrent geographic pattern on the six maps. However, according to the diagnoses, some geographic contrasts can be noticed. In the Southwest of France, there is a slight underestimation of the standard deviation and P90, an overestimation of P10, the correlation coefficients are lower, but the RMSE and the mean wind speed errors remain weak. In the regions that exhibit high wind speed variability, namely the coastal areas in the Northwest and the Southeast, the RMSE is higher while there is high correlation coefficients. In most stations of the South of

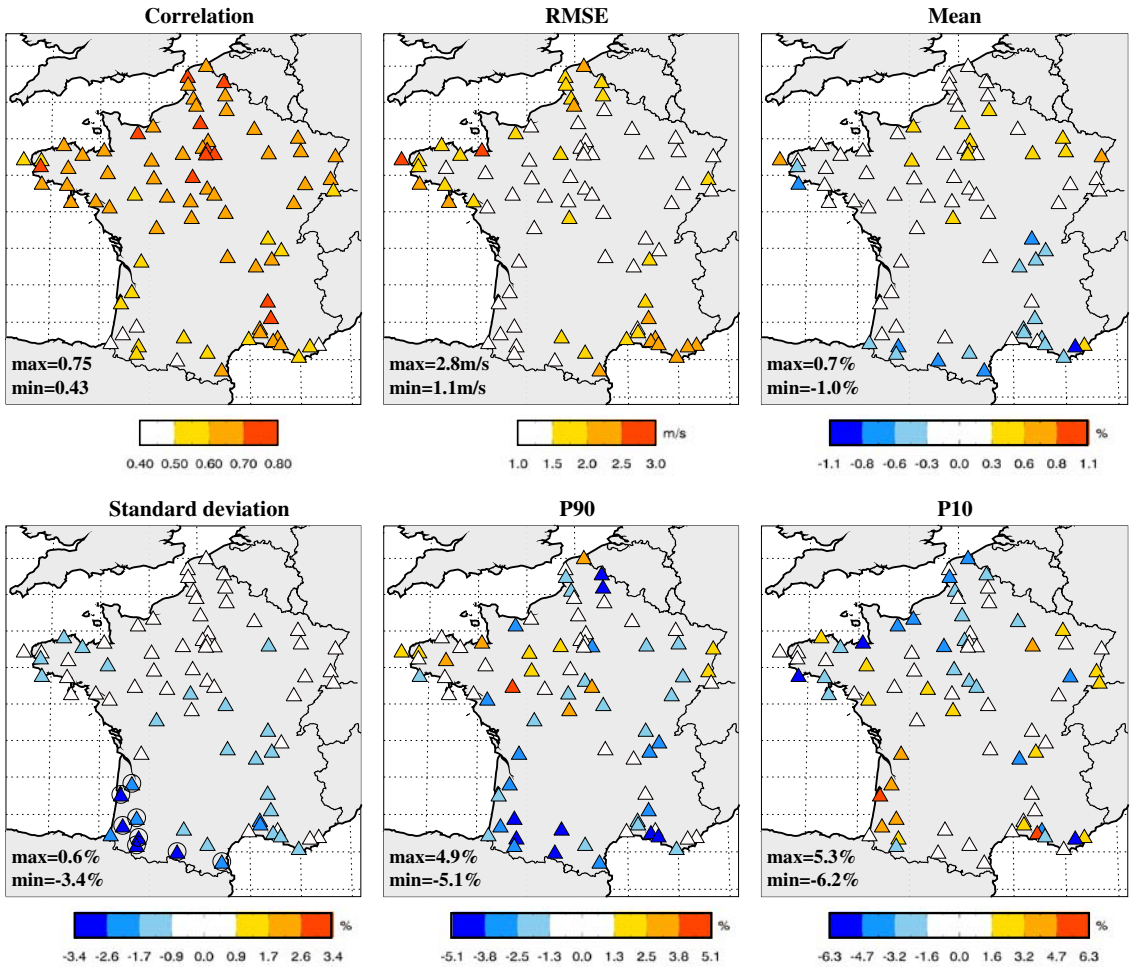

Fig. 6 Daily linear correlations (*upper left panel*), RMSE (*upper central panel*), mean errors (*upper right panel*—in percent), standard deviation errors (*lower left panel*—in percent), 90th percentile errors (P90) (*lower central panel*—in percent) and 10th percentile (P10) errors (*lower right panel*—in percent) between observed and downscaled daily wind speeds for each station (1974–2002). The large circles indicate stations where errors are significant at the 0.05 level (Wilcoxon Rank-Sum test for the mean and *F*-statistic test for the standard deviation). Correlation coefficients are significant at the 0.05 level (''random-phase'' test accounting for autocorrelation described in Ebisuzaki 1997)

France, there is a slight underestimation of the mean wind speed, standard deviation and P90. As said previously, results are similar for both the cold and warm seasons. However, while the spatial patterns of the results are almost identical, daily linear correlation coefficients are higher for the cold season, and RMSE and mean errors are slightly weaker for the warm season (not shown).

In order to assess the performance of our method for the six diagnoses presented previously, it is has been confronted to three other downscaling algorithms: two linear regression methods and an analog method. The analog method (called Anal) is implemented in the EOF state space as described by Zorita and von Storch (1999). The first linear regression method (called Reg_WT) consists in performing linear regressions at each station between the observed wind speeds and the Euclidean distances to the weather type centroids (this is exactly similar to our method without the final reconstruction step—see Sect. 3.3). The second linear regression method (called Reg_EOF) consists in performing linear regressions at each station between the observed wind speeds and the principal component coefficients. Table 1 shows the performance of each method for the 6 diagnoses presented in Fig. 6. For daily linear correlation, RMSE and mean error, the Reg_WT method provides the best results. Differences between the other methods are small and none of them distinguishes itself from the others. Concerning wind speed distribution features (standard deviation, P90, P10), our method outperforms the other ones. Note that as no inflation method has been applied to the linear regression methods, they largely underestimate the variance and P90, and overestimate P10. Finally, as the ability to reproduce the main wind speed distribution features is essential for impact studies, it appears that our method provides a good

Table 1 Daily linear correlations, RMSE, mean errors, standard deviation (SD) errors, 90th percentile errors (P90) and 10th percentile (P10) errors between observed and downscaled daily wind speeds averaged in absolute value over all stations (1974–2002). WT indicates our method, Reg_WT indicates the linear regression method with the distances to the weather type centroids, Reg_EOF indicates the linear regression method with the principal component coefficients, Anal indicates the analog method

	Correlation	RMSE (m/s)	Mean (%)	SD (%)	P90 (%)	P10 (%)
WT	0.63	1.59	0.3	0.9	2.0	2.0
Reg_WT	0.77	1.19	0.1	21.8	35.6	81.3
Reg_EOF	0.56	1.54	0.1	42.5	75.0	83.3
Anal	0.67	1.48	2.4	3.8	11.7	4.9

compromise between all diagnoses. Furthermore, we also compared the spatial patterns of the errors obtained with the four methods (not shown). We found that all methods lead to geographic contrasts, which are similar to the ones described previously for most cases.

Next, Fig. 7 shows the monthly mean annual cycle of the observed and downscaled wind speeds at two stations which exhibit different annual cycles, and are good representatives of two regions of interest for wind energy: Station 27 on the western Atlantic coast and Station 63 in southeastern France. Once more, the downscaling method provides results which are in good agreement with observations. This is particularly interesting as the monthly mean wind speed annual cycle is very different at these stations: while it is weak in Station 63 (with a small increase of the mean wind speed in spring), the seasonal cycle is quite strong in Station 27. As shown in Fig. 8, the monthly mean annual cycle is actually properly reproduced in most stations: the mean absolute error in percent averaged over all stations is equal to 3.9%. The highest discrepancies are found in the Southwest.

The last evaluation relates to the temporal evolution of extreme wind speed indices. Figure 9 shows the number of days per year for which the wind is higher than 15.9 m/s (95th percentile of the observed daily maximum over France of the daily 10 m wind speed) in at least one station, according to the observed and downscaled wind speeds. It can be seen that the inter-annual variability is properly reproduced, the linear correlation coefficient between the downscaling results and the observations being equal to 0.67 (significant at the 0.05 level).

To conclude, the downscaling method shows good skills in reproducing a large number of wind speed features. The different diagnoses that have been presented show weak differences between reconstructed and observed wind speeds (most of the differences are not statistically significant).

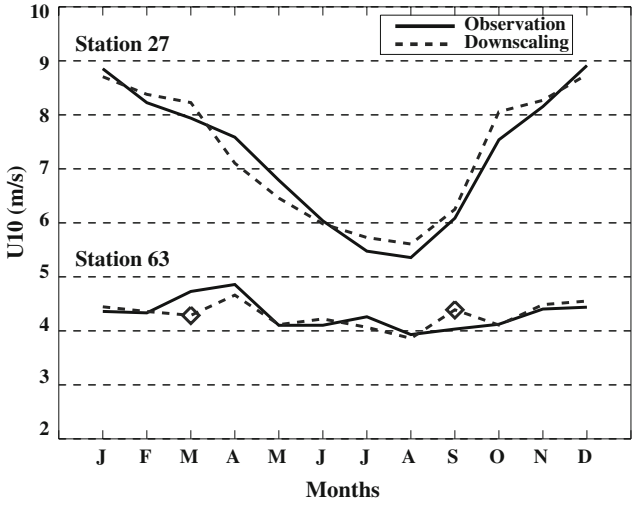

Fig. 7 Monthly mean annual cycle of the observed and downscaled wind speeds (1974–2002) at Station 27 on the western Atlantic coast and Station 63 in southeastern France. *Black solid lines* indicate observations, *dark-gray dashed lines* indicate the downscaling method. *Diamonds* indicate months where differences are significant at the 0.05 level (Wilcoxon Rank-Sum test)

5 Future climate

5.1 Methodology

We use the 850 hPa winds from the 14 CMIP3 models as predictors (see Sect. 2.3). The *UV*850 anomalies are

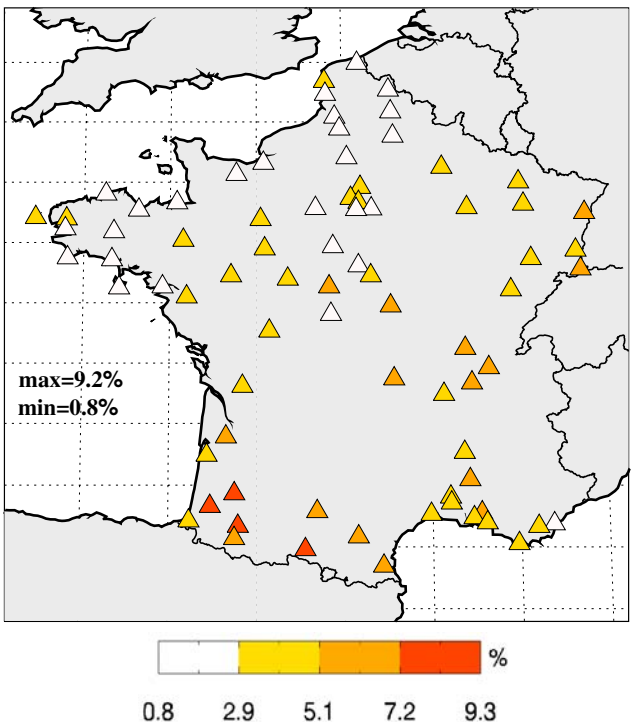

Fig. 8 Mean absolute errors in percent between the downscaled and observed monthly mean annual cycles (1974–2002)

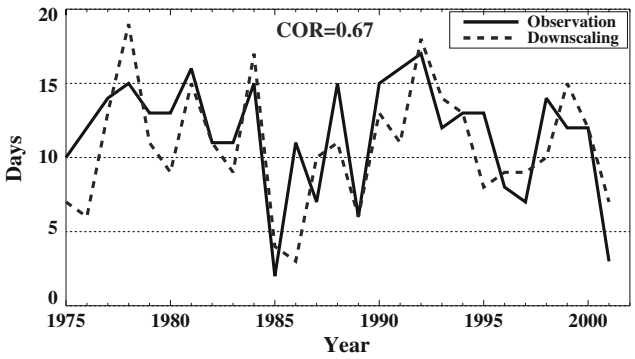

Fig. 9 Number of days per year for which the wind is higher than 15.9 m/s in at least one station (95th percentile of the daily maximum over France of the daily 10 m wind speed), according to the observed and downscaled wind speeds (1974–2002). *Black solid lines* indicate observations, *dark-gray dashed lines* indicate the downscaling method. Correlation coefficients are significant at the 0.05 level (''random-phase'' test accounting for autocorrelation described in Ebisuzaki 1997)

computed using the historical period climatologies. Then, the *UV*850 anomalies are projected onto the learning period ERA40 *UV*850 EOFs, and classified in the weather types by minimization of the distance to the ERA40 *UV*850 weather type centroids. Finally, the downscaling algorithm is performed for both the cold and warm seasons.

5.2 Historical period

5.2.1 Predictor validation

According to our methodology, we need to ensure that the CMIP3 models reproduce adequately the main features of the weather types.

First of all, the ability of the models to properly reproduce the *UV*850 mean states within the weather types is assessed by means of Taylor diagrams (Taylor 2001, Fig. 10). Those diagrams provide a concise statistical summary of how well spatial patterns match each other in terms of their correlation, their root-mean-square difference and the ratio of their variances. First of all, it can be seen that the pattern correlations are generally high (higher than 0.6 in most cases). Secondly one can notice that the variance is generally underestimated by the models, whatever the weather type or the season. This was actually expected. Indeed most models have horizontal resolution lower than the ERA40 resolution, therefore the spatial variability of the interpolated fields is smaller for most models. It is also interesting to note that there is high coherence between the models: they share similar qualities or deficiencies (see the clusters of color points).

Then, we compare the occurrence frequencies of the weather types when classifying the *UV*850 from ERA40 and the CMIP3 models for the historical period (see Fig. 11). Results with the CMIP3 models are generally close to the reanalysis, except for $WT2_{cold}$ for the cold season and $WT1_{warm}$ for the warm season: $WT2_{cold}$ occurrence is underestimated by the CMIP3 models and there is low dispersion of the models, while $WT1_{warm}$ is generally overestimated by the CMIP3 models and there is high dispersion of the models.

5.2.2 Downscaling validation

We now compare the multi-model downscaled 10 m wind speeds using the CMIP3 predictors with the observations over the period 1974–2000. As is shown in Fig. 12, although errors are slightly larger than for the cross-validation with the ERA40 predictors, results remain satisfactory. However, it can be seen that the multi-model 10 m wind speeds and standard deviations are overestimated in the Southeast and underestimated in the North. The same pattern is found for both seasons. We found that other downscaling methods lead to the same pattern. In order to investigate the sources of this pattern, we have conducted a similar study as in Sect. 5.3.2 (not shown). We found that only a small fraction of this bias originates from errors in the weather type occurrences, except for the warm season, for which the overestimation of the $WT1_{warm}$ occurrence and the slight underestimation of the $WT3_{warm}$ occurrence contributes to this pattern. Actually, most of this bias originates from an underestimation of the 10 m wind speeds in the Northwest of France for $WT4_{cold}$ and $WT6_{cold}$ for the cold season, and $WT4_{warm}$ and $WT5_{warm}$ for the warm season.

5.3 Climate scenario

5.3.1 Downscaled wind speeds

We now focus on the climate projection periods 2046–2065 and 2081–2100 (see Sect. 2.3). Results of the SD for those two periods are compared with results for the historical period (Figs. 13, 14, 15, and 16).

For the cold season (Fig. 13), the Mediterranean area experiences a decrease of the mean wind speed, while northwestern France experiences a weak increase. Those changes are larger for the 2081–2100 period than for the 2046–2065 period. In the Southeast, there is good agreement between the models with regard to the sign of the changes. Indeed at least 80% of the models provide changes of the same sign. On the contrary, in the North (except the most northern part) and the Center there is little sign coherence between the models. Furthermore, the lower panels of Fig. 13 show that the inter-model dispersion is weak in the Mediterranean area and larger in the

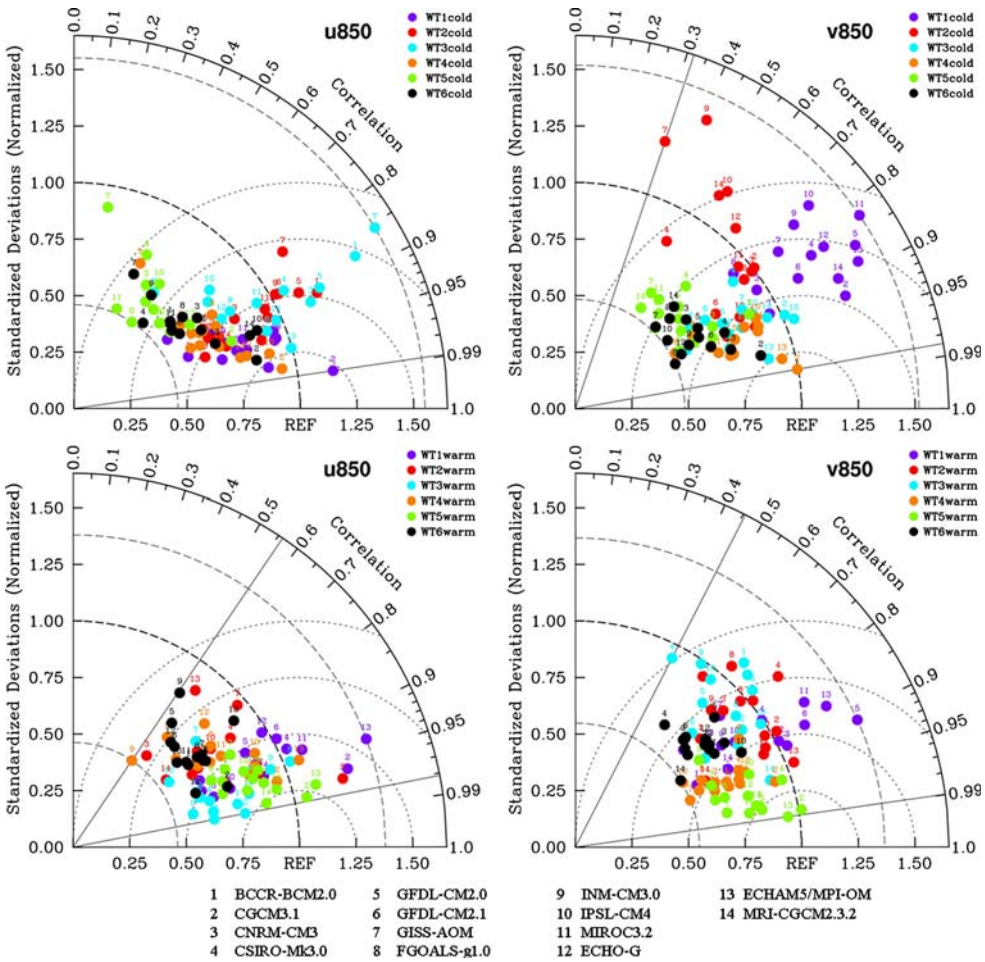

Fig. 10 Taylor diagram for the mean zonal (*left panel*) and meridional (*rignt panels*) 850 hPa wind components of each weather type for the cold season (*upper panels*) and the warm season (*lower panels*) of the historical period (1971–2000). The horizontal and vertical axes represent the ratio of the standard deviations of the reference (ERA40) and simulated (CMIP3) fields. The radial axis indicates the spatial correlation between the reference and simulated fields. The distance between the origin (noted REF) and any point is proportional to the RMSE

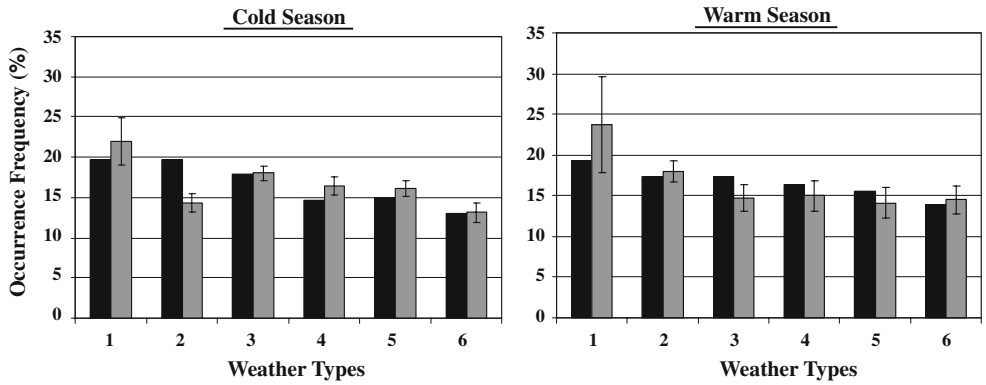

Fig. 11 Weather type occurrences in percent for each season when classifying the 850 hPa wind fields from ERA40 (*black*) and the CMIP3 models (*dark-gray*) (occurrences averaged over all the CMIP3 models) for the historical period 1971–2000. Classification is performed in the space spanned by the learning period ERA40 850 hPa wind field EOFs using the centroids of the learning period weather types (1974–2002). *Vertical bars* represent the dispersion of the models (±1 inter-model standard deviation)

North of France. However, the amplitude of the multi-model mean changes are only significantly larger than the inter-model dispersion in the Southeast and for the 2081–2100 period only (2 times larger on average). Concerning extreme wind speed indices (Fig. 14), the number of high wind days decreases near the Mediterranean Sea and increases in northwestern France, while the number of low wind days increases significantly near the Mediterranean Sea.

For the warm season (Fig. 15), the mean wind speed decreases in most stations. Those changes are larger for the 2081–2100 period than for the 2046–2065 period. The sign

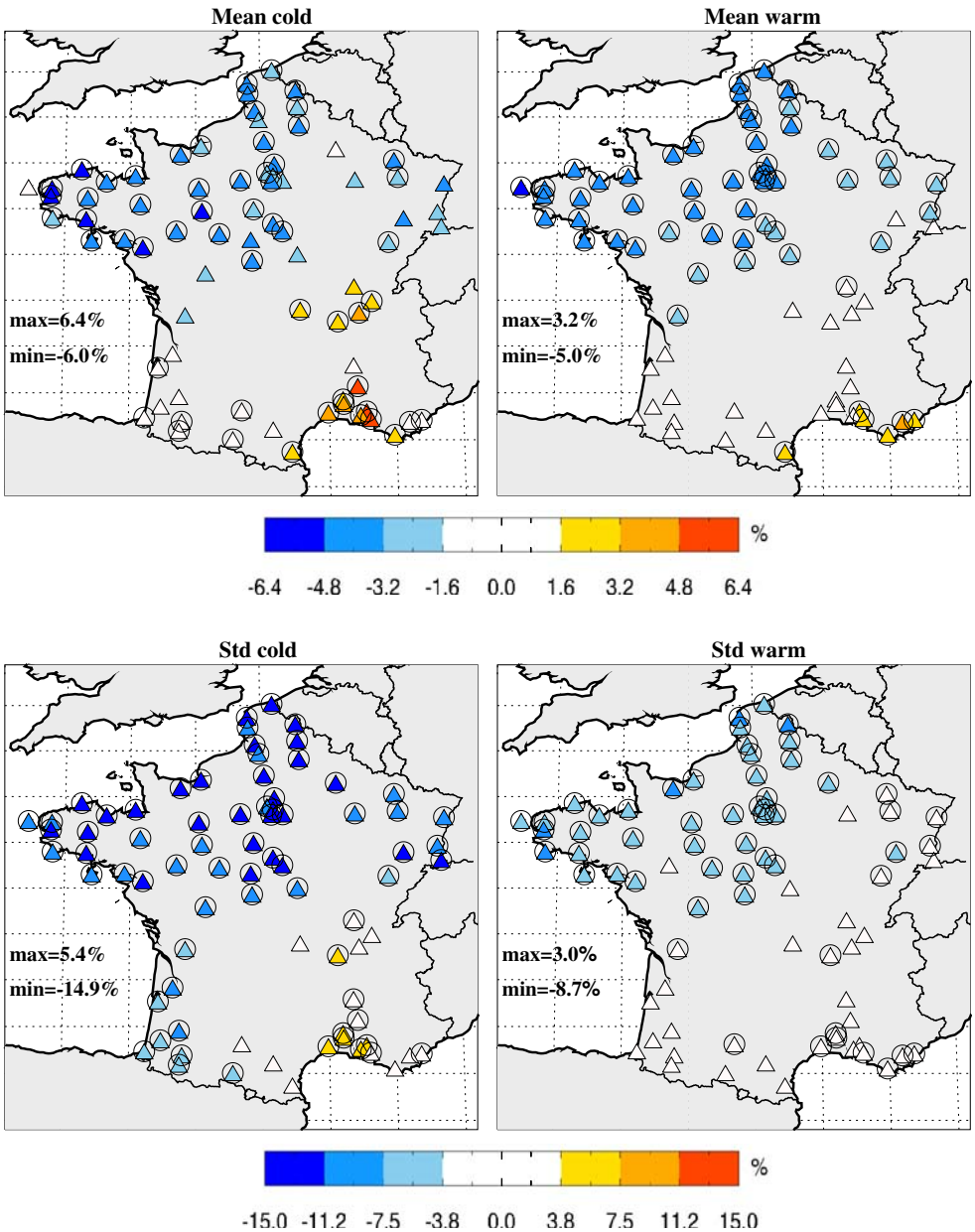

Fig. 12 Multi-model mean error (*upper panels*) and standard deviation error (*lower panels*) between observed and downscaled 10 m wind speeds over the period 1974–2002 for the cold season (*left panels*) and the warm season (*right panel*), formulated as percentages of the observed wind speed and the observed wind speed standard deviation, respectively. The large circles indicate the stations where the errors are significant at the 0.05 level (Wilcoxon Rank-Sum test for the mean and *F*-statistic test for the standard deviation)

coherence of the models is high in most stations (at least 80% of the models provide changes of the same sign in most stations) and the inter-model dispersion is weak all over France except in the Southeast. The amplitude of the multimodel mean changes are significantly larger than the inter-model dispersion in the West and the center of France for both periods. These changes in the mean wind speed are reinforced by a strong decrease of the number of high wind days and a strong increase of the number of low wind days all over France (Fig. 16).

For all seasons and variables (mean wind speed, *N*90, *N*10), the sign coherence of the models increases between 2046–265 period and the 2081–2100 period, while the dispersion increases in most stations. As a consequence, although the agreement between the models increases with time with regard to an increase or a decrease of mean wind speed, *N*10 and *N*90, the agreement with regard to the magnitude of those changes decreases with time.

For both seasons and periods, multi-model mean 10 m wind speed changes remain weak (maximum of 5.7%). However, those changes are statistically significant. Furthermore, changes in *N*10 and *N*90 are of much larger magnitude (maximum of 21.5%), and changes in the multi-model mean wind power density (which is proportional to the cube of the wind speed) are also much larger (maximum of 18%) (not shown).

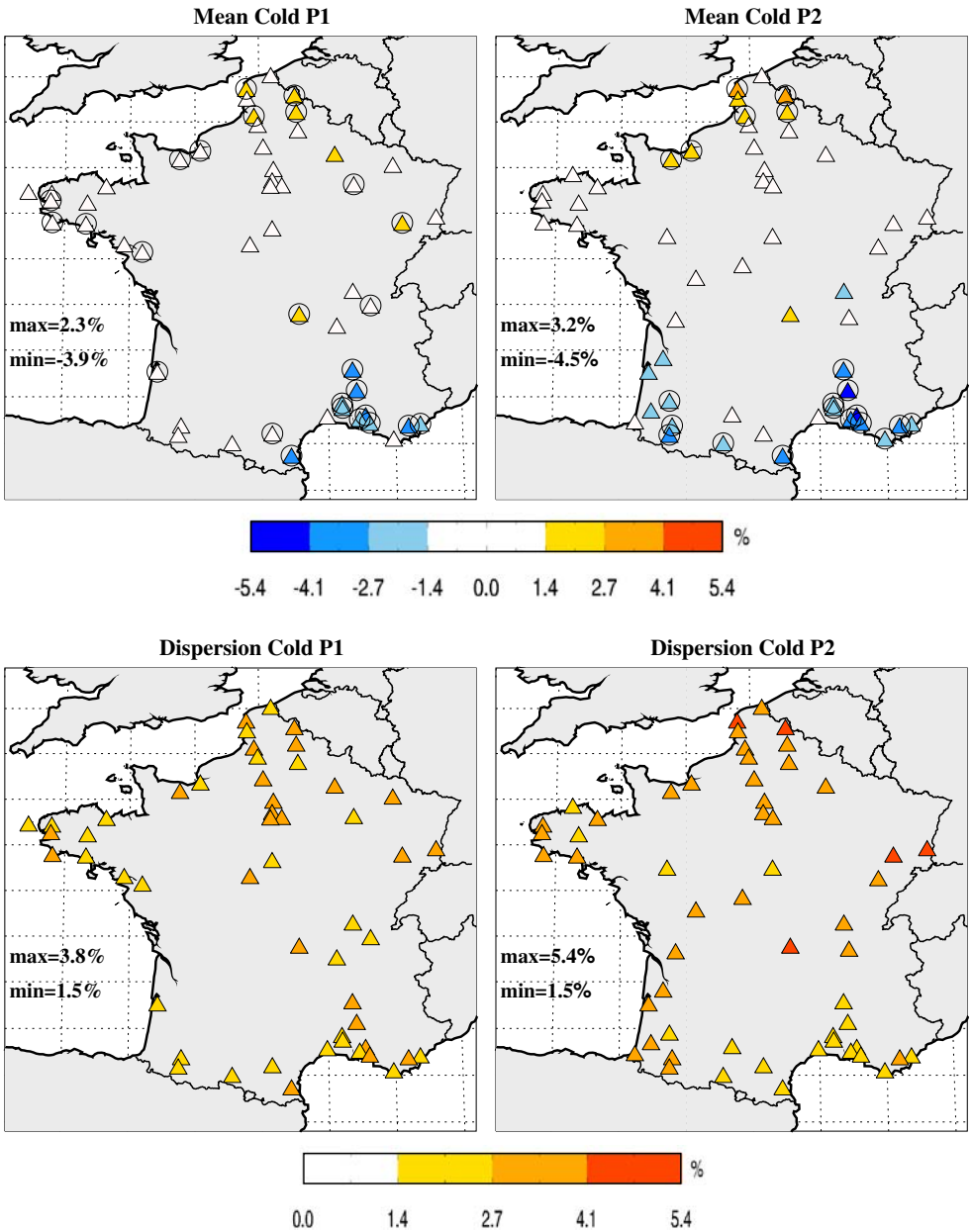

Fig. 13 *Upper panels*: multi-model mean 10 m wind speed changes (in percent) for the cold season, between 2046–2065 and 1971–2000 (*left panel*) and between 2081–2100 and 1971–2000 (*right panel*). Only stations where differences are significant at the 0.05 level are shown (Wilcoxon Rank-Sum test). The large circles indicate the stations where at least 80% of the models (11 over 14) provide changes of the same sign. *Lower panels*: One inter-model standard deviation (in percent)

5.3.2 *Intertype and intratype changes*

The changes in the 10 m wind speeds that have been highlighted previously may be explained in terms of weather type modifications: this is one of the assets of the weather type downscaling method. Modifications of the weather types may occur in two ways: modification of the distribution of the days within the weather types (intratype modification) and modification of the weather type occurrences (intertype modification).

We first investigate the evolution of the weather type occurrences (intertype approach). The relevance of this approach relies on recent studies which suggested that anthropogenic climate change may manifest itself as a projection onto the preexisting natural modes of variability of the climate system (Corti et al. 1999; Stone et al. 2001).

As illustrated in Fig. 17, significant changes occur for the cold season: $WT1_{cold}$ occurrence increases by 8 and 12% and $WT4_{cold}$ occurrence by 11 and 11%, while $WT2_{cold}$ occurrence decreases by 13 and 14% and $WT5_{cold}$ occurrence by 10 and 14% (percentages of increase/decrease relative to the occurrence frequencies in the historical simulation). Note that those results agree with previous studies concerning changes in the residence frequency of the climate system in the wintertime North Atlantic-European atmospheric circulation regimes (Terray et al. 2004; Stephenson et al. 2006). Those changes in the

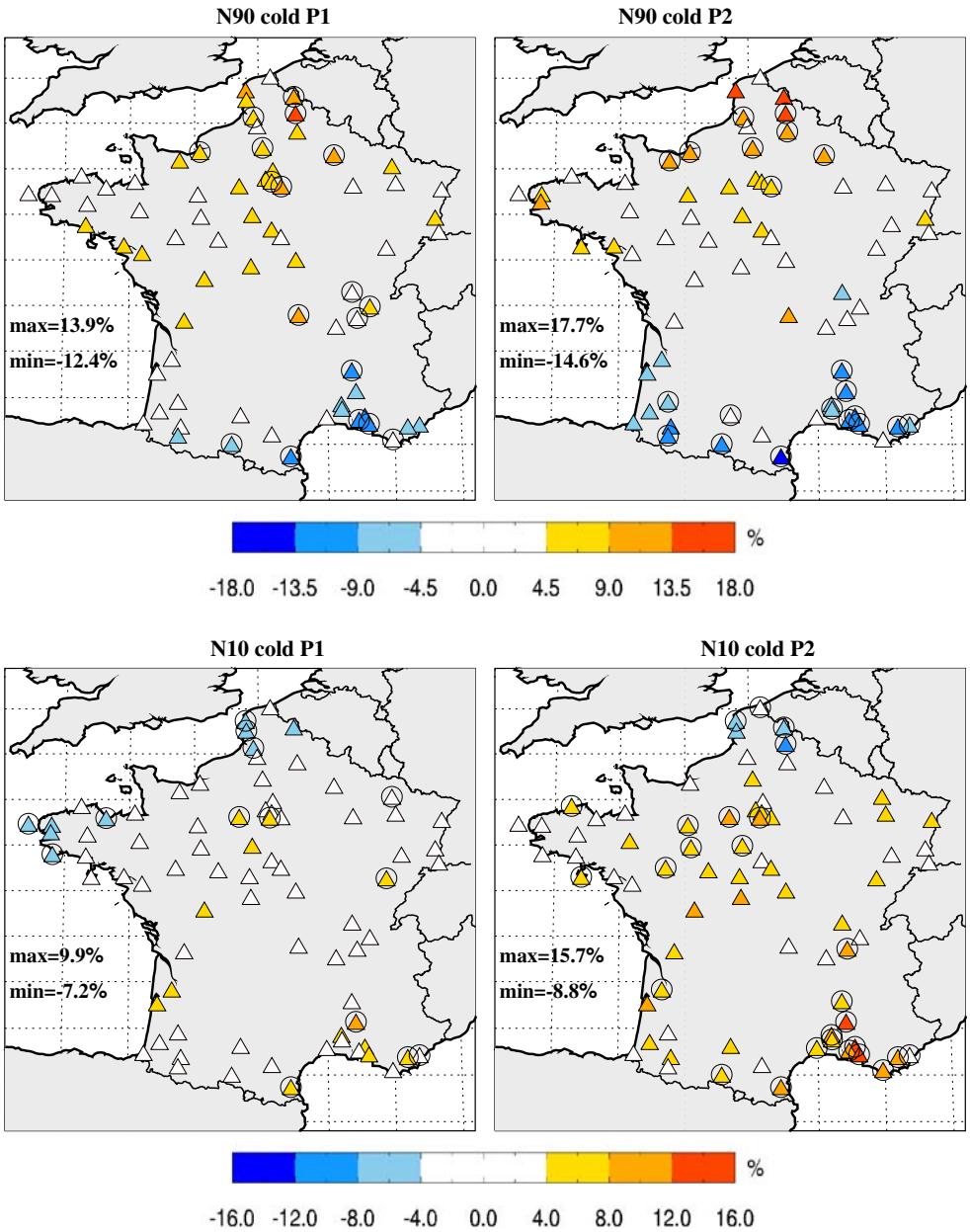

Fig. 14 *Upper panels*: multi-model changes in some extreme 10 m wind speed indices. *Upper panels*: multi-model mean changes in the number of high wind days (*N*90) (in percent). High wind days are defined at each station and occur when the mean 10 m wind speed is higher than the 90th percentile (P90) of the historical period daily mean 10 m wind speed. *Lower panels*: multi-model mean changes in the number of low wind days (*N*10) (in percent). Low wind days are defined at each station and occur when the mean 10 m wind speed is lower than the 10th percentile (P10) of the historical period daily mean 10 m wind speed. *Left panels*: multi-model mean changes between 2046–2065 and 1971–2000. *Right panels*: multi-model mean changes between 2081–2100 and 1971–2000. Only stations where differences are significant at the 0.05 level are shown. The *large circles* indicate the stations where at least 80% of the models (11 over 14) provide changes of the same sign

weather type occurrences may have additive effects and give rise to important changes in the wind speed distribution. Indeed, according to Sect. 4.1 and Fig. 3, $WT4_{cold}$ is associated with strong southwesterly winds in northern France, $WT1_{cold}$ with weak anticyclonic winds over France, $WT5_{cold}$ with weak northerly winds in northern France and strong wind events in the Mediterranean area (Mistral and Tramontana), and $WT2_{cold}$ with weak northeasterly winds all over France. As a consequence, for the cold season, changes in the weather type occurrence are expected to lead to a decrease of the wind speed in the Mediterranean area and an increase in northwestern France. This is in perfect agreement with the 10 m wind speed changes highlighted in Sect. 5.3.1.

For the warm season, $WT1_{warm}$ occurrence increases by 14 and 22%, while $WT2_{warm}$ occurrences decrease by 11 and 14% and $WT5_{warm}$ occurrences decrease by 9 and 16%. According to Sect. 4.1 and Fig. 4, $WT1_{warm}$ is associated with weak anticyclonic winds over France, $WT2_{warm}$ with southerly winds all over France and $WT5_{warm}$ with strong southwesterly winds in northern France. As a result, changes in the weather type occurrences for the warm season are expected to lead to a low decrease of the wind speed all over France. This is also in agreement with the 10 m wind speed changes highlighted in Sect. 5.3.1.

However, changes in the weather type occurrences may not be sufficient to draw any firm conclusion concerning

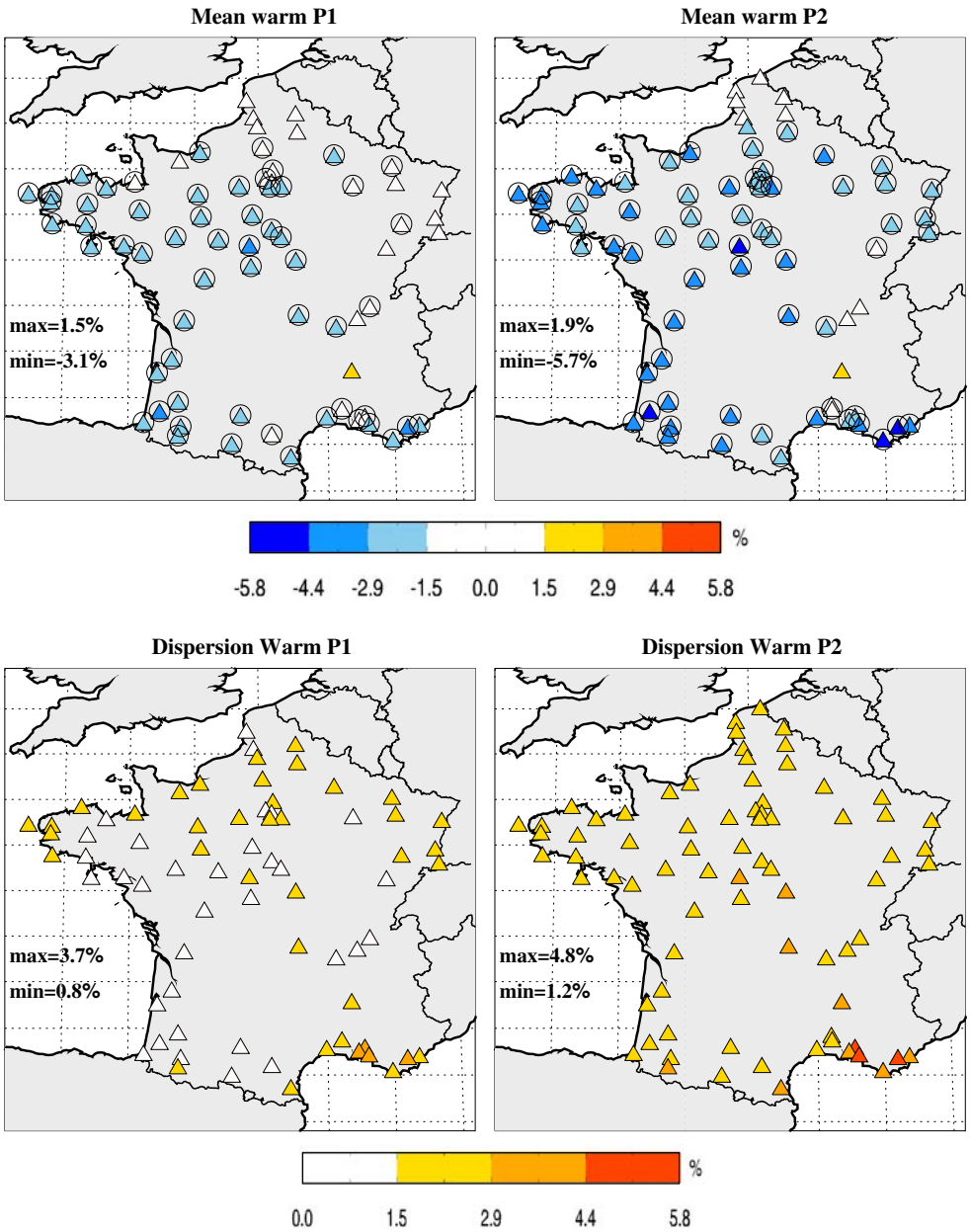

Fig. 15 Multi-model mean 10 m wind speed changes and model dispersion for the warm season. See legend of Fig. 13

the downscaled wind speed, as changes in the distribution of the days within the weather types may be as much or even more important. In order to quantify the effects of the intratype and intertype modifications separately, we follow Boé et al. (2006) and use a simple mathematical decomposition of the total anomaly ΔX of a regional variable between future and present climate:

$$\Delta X = X^{\mathrm{f}} - X^{\mathrm{p}} = \sum_{j=1}^{N} \left(f_j^{\mathrm{f}} \cdot x_j^{\mathrm{f}} - f_j^{\mathrm{p}} \cdot x_j^{\mathrm{p}} \right) \quad (1)$$

where, X^{p} (X^{f}) is the mean value of a regional variable in present (future) climate, N is the number of weather types, f_j^{p} (f_j^{f}) is the occurrence frequency of the jth weather type in present (future) climate, and x_j^{p} (x_j^{f}) is the mean value of the regional variable in the jth weather type in present (future) climate.

Equation 1 can be rewritten as:

$$\Delta X = \sum_{j=1}^{N} \left(f_j^{\mathrm{f}} - f_j^{\mathrm{p}} \right) x_j^{\mathrm{p}} + f_j^{\mathrm{p}} \left(x_j^{\mathrm{f}} - x_j^{\mathrm{p}} \right) + \left(f_j^{\mathrm{f}} - f_j^{\mathrm{p}} \right) \left(x_j^{\mathrm{f}} - x_j^{\mathrm{p}} \right) \quad (2)$$

Finally, we can exhibit three terms:

$$\Delta X = \sum_{j=1}^{N} \left(\Delta f_j \cdot x_j^{\mathrm{p}} \right) + \sum_{j=1}^{N} \left(f_j^{\mathrm{p}} \cdot \Delta x_j \right) + \sum_{j=1}^{N} \left(\Delta f_j \cdot \Delta x_j \right) \quad (3)$$

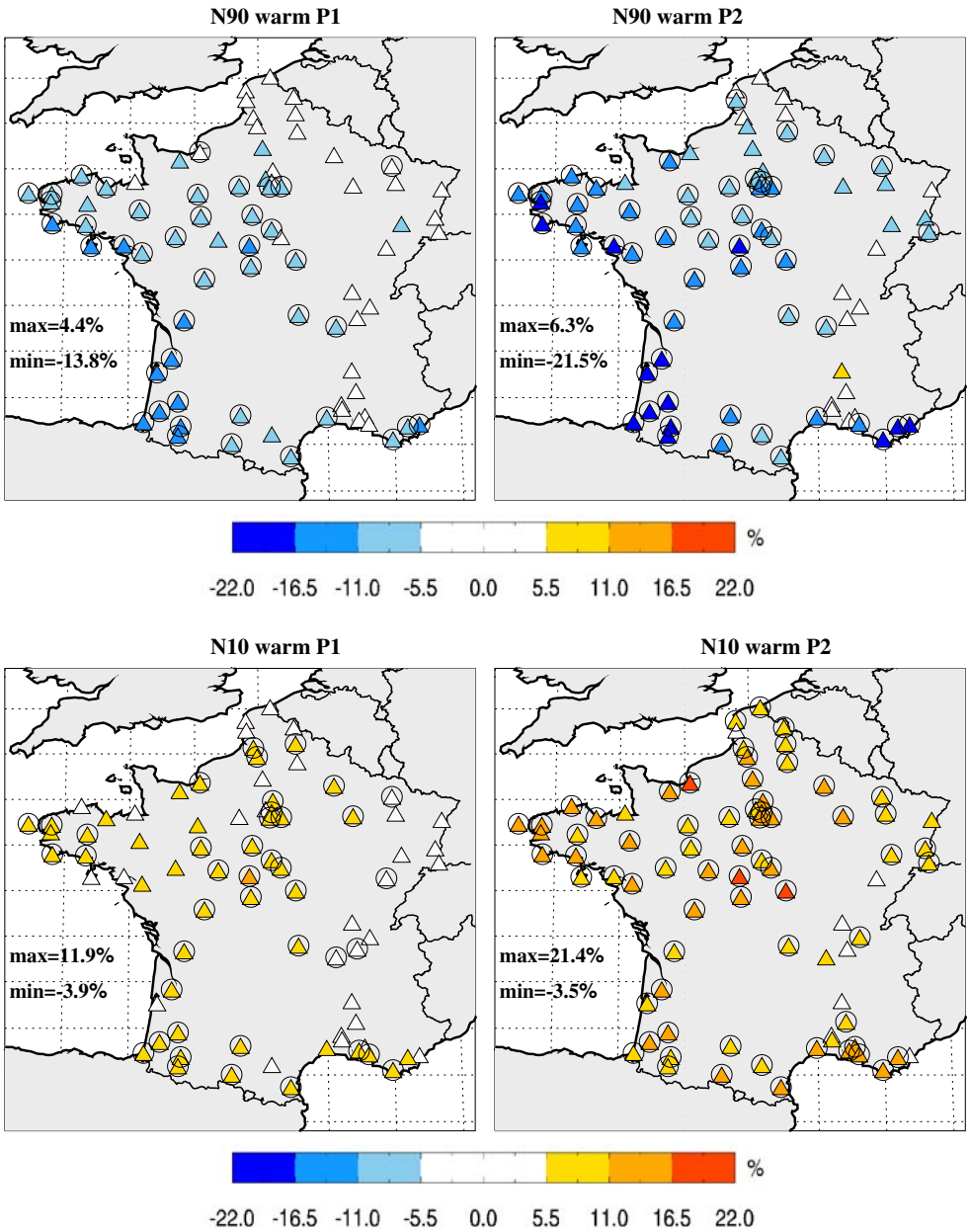

Fig. 16 Multi-model changes in some extreme 10 m wind speed indices for the warm season. See legend of Fig. 14

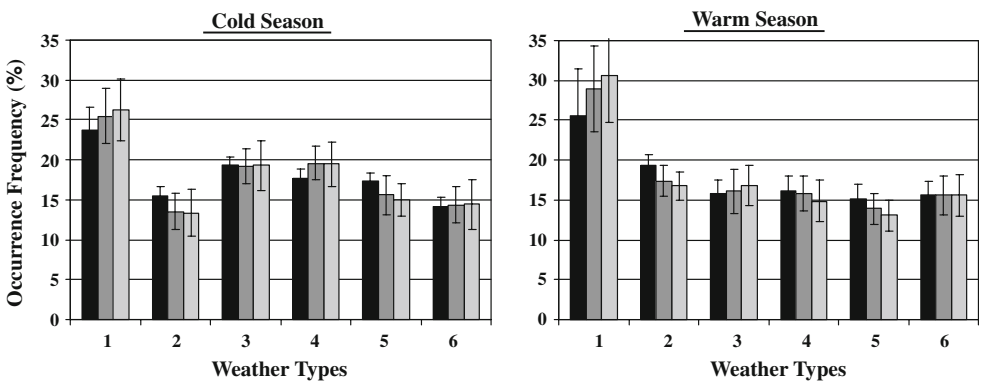

Fig. 17 Weather type occurrence frequencies (averaged over all the CMIP3 models) in percent for the cold and warm seasons, for the historical period (*black*), 2046–2065 (*dark-gray*) and 2081–2100 (*light-gray*). *Vertical bars* represent the dispersion of the models (±1 inter-model standard deviation)

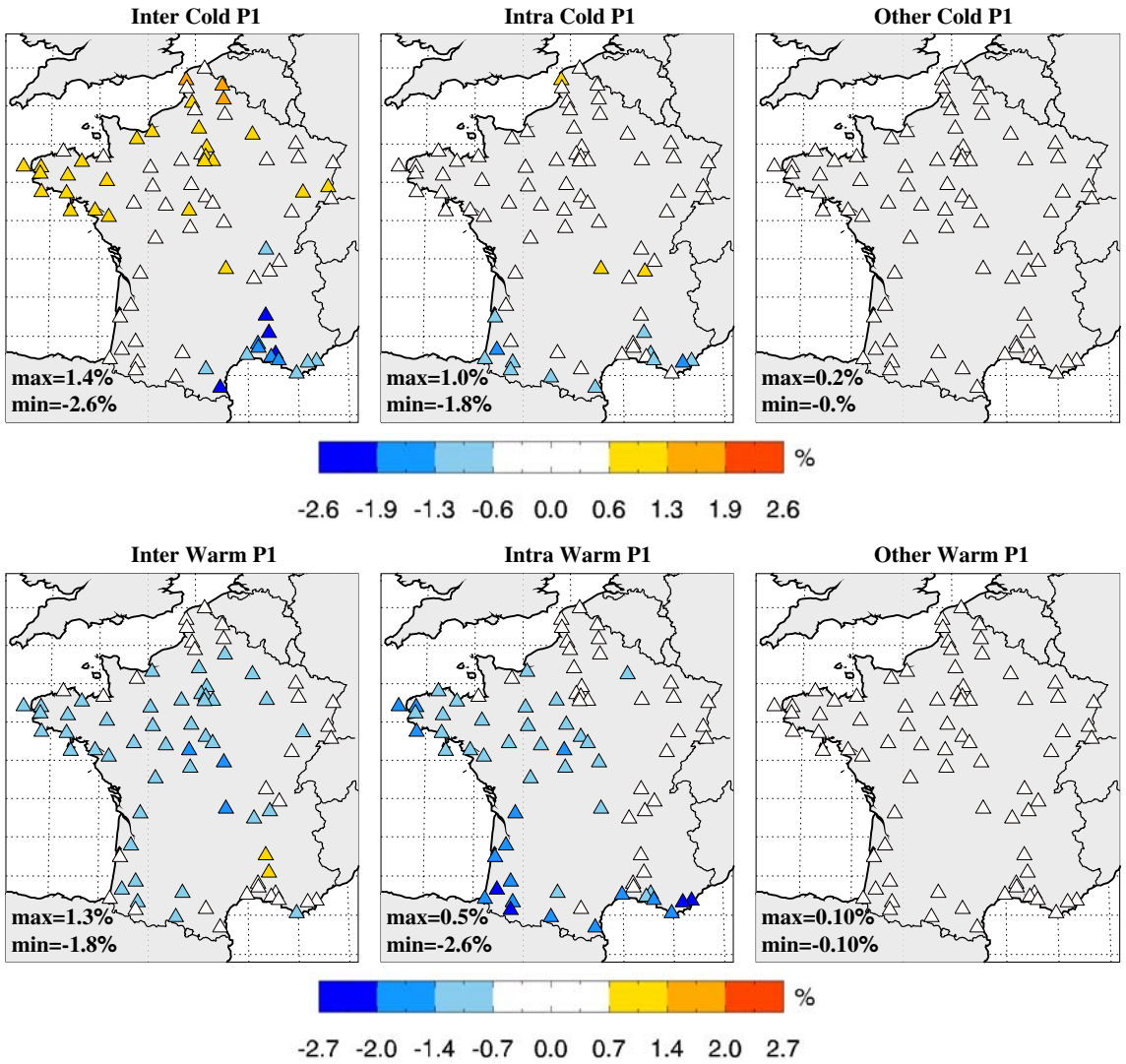

Fig. 18 Effects of the different terms of the 10 m wind speed anomaly decomposition (see Eq. 3) upon the mean 10 m wind speed for the 2046–2065 period (formulated as percentages of the mean 10 m wind speed over the historical period (1971–2000)). The three terms of Eq. 3 have been evaluated for each model, and the average of each term over all models is presented. *Upper* (*lower*) panels show results for the cold (warm) season. Effects of the intertype modifications are shown on the *left panels*, effects of the intratype modifications are shown on the *center panels*, and effects of the other modifications are shown on the *right panels*. Results are to be confronted with results in Figs. 13 and 15 for the 2046–2065 period

where $\Delta x_j = x_j^{\mathrm{f}} - x_j^{\mathrm{p}}$ and $\Delta f_j = f_j^{\mathrm{f}} - f_j^{\mathrm{p}}$.

The first term of Eq. 3 represents the part of the total anomaly that is due to changes in the occurrence frequency of the weather types: this is the intertype change. The second term represents the part of the total anomaly that is due to changes within weather types: this is the intratype change. The third term exhibits both the intertype and intratype changes.

We have applied this decomposition to the 10 m wind speed. As shown in Fig. 18 for the 2046–2065 period, the third term of Eq. 3 is much smaller than the first and second terms. Furthermore, the intertype and intratype changes are generally of similar magnitude. For the warm season, they are of the same signs in most stations and the intratype changes slightly dominate in the South. For the cold season, intertype and intratype changes of the same sign in the Mediterranean area while they are of opposite signs in the West and North of France. The intertype changes dominate in the North and the Southeast. Finally, the intratype modifications play a role as important as the intertype modifications in the 10 m wind speed changes. In some cases like the Mediterranean area for the cold season or most of France for the warm season, the effects of the intertype and intratype modifications add up, resulting in a

significant decrease of the 10 m wind speeds. On the contrary, in the North and West of France the intratype modifications countered the intertype modifications. Results for the 2081–2100 period are similar, except that changes are stronger (up to 4.4%) (not shown). These results show that changes in the weather type occurrences are only a part of the climate change signal and are not sufficient to explain the whole change in the 10 m wind speeds.

6 Conclusion

In this paper we have presented a statistical downscaling method for 10 m wind speeds over France. We performed a cross-validation of the method over the whole learning period (1974–2002). Good agreements with the observations were pointed out. We applied the method with predictors from 14 AOGCMs. For the cold season, we found significant changes in the Southeast (decrease of the mean wind speed and the number of high wind days, and an increase in the number of low wind days) and in the North (increase in the mean wind speed and the number of high wind days, and decrease of the number of low wind days). For the warm season, we found significant changes all over France with a decrease of the mean wind speed and the number of high wind days, and an increase of the number of low wind days in all stations. For both seasons, changes are larger for 2081–2100 than for 2046–2065. We found good agreement between the models with regard to the sign of the changes in most stations for the warm season, and in a few stations for the cold season. Moreover, the magnitude of the changes remains uncertain in most cases as the inter-model dispersion is of the same order of magnitude as the amplitude of the changes. Finally, we showed that those changes are due to both intratype and intertype modifications.

Concerning wind energy applications, those results show that the North of France may experience an increase of its wind energy ressources during the cold season and a decrease during the warm season, while the Southeast may expect a decrease of its wind energy ressources during both the cold and warm season. Given the fact that the coastal areas of those regions are among the most attractive locations for wind energy in Europe (Troen and Petersen 1989), those results may be of interest for wind energy development in France.

Finally, the SD method developed in this paper is well adapted to impact studies using multi-model ensembles. The current version of the method remains simple: only one predictor, a few weather types, and linear regressions. Besides, the construction of the method enables to get physical interpretations of each step: weather types and atmospheric dynamics, linear regressions, and intratype variability, intratype and intertype modifications under perturbed climate.

As a conclusion, it is worth pointing out that this method may be easily implemented for probabilistic forecasting for a wide range of time scales: from daily forecasting to future climate study, and monthly and seasonal forecasting. Furthermore, in order to overcome the low density of stations over France, future work will consist in associating the SD method to mesoscale modeling so that high spatial resolution results will be provided for some areas of interest.

Acknowledgments J. Najac Ph.D. grant was partly supported by Electricité de France (EDF). ECMWF ERA-40 data were obtained from the ECMWF data server. The authors are grateful to the Division de la Climatologie (DCLIM) at Météo-France for providing the SQR dataset. We acknowledge the modeling groups, the Program for Climate Model Diagnosis and Intercomparison (PCMDI) and the WCRP's Working Group on Coupled Modeling (WGCM) for their roles in making available the WCRP CMIP3 multi-model dataset. Support of this dataset is provided by the Office of Science, U.S. Department of Energy. Some statistical calculations have been performed with Statpack, developed by P. Terray (IPSL/LOCEAN). We would like to thank S. Parey, C. Fil-Tardieu and C. Cassou for stimulating discussion about this work, and the anonymous reviewers for their constructive comments which helped to improve this article.

References

Alexander LV, Tett SFB (2005) Recent observed changes in severe storms over the United Kingdom and Iceland. Geophys Res Lett 32:L13704. doi:10.1029/2005GL022371

Archer CL, Jacobson MZ (2005) Evaluation of global wind power. J Geophys Res 110:D12110. doi:10.1029/2004JD005462

Bärring L, von Storch H (2004) Scandinavian storminess since about 1800. Geophys Res Lett 31:L20202. doi:10.1029/2004GL020441

Boé J, Terray L, Habets F, Martin E (2006) A simple statistical-dynamical downscaling scheme based on weather types and conditional resampling. J Geophys Res 111:D23106. doi:10.1029/2005JD006889

Bogardi I, Matyasovszky I (1996) Estimating daily wind speed under climate change. Solar Energy 57-3:239–248

Cassou C, Terray L, Phillips AS (2005) Tropical Atlantic influence on European heatwaves. J Clim 18:2805–2811. doi:10.1175/JCLI3506.1

Cleugh HA, Miller JM, Bohm M (1998) Direct mechanical effects of wind on crops. Agrofor Syst 41:85–112. doi:10.1023/A:1006067721039

Conil S, Hall A (2006) Local modes of atmospheric variability: a case study of southern California. J Clim 19-17:4308–4325

Corti S, Molteni F, Palmer TN (1999) Signature of recent climate change in frequencies of natural atmospheric circulation regimes. Nature 398:799–802. doi:10.1038/19745

Ebisuzaki W (1997) A method to estimate the statistical significance of a correlation when the data are serially correlated. J Clim 10–9:2147–2153

Fisher-Bruns I, von Storch H, Gonzales-Rouco JF, Zorita E (2005) Modeling the variability of midlatitude storm activity on decadal to century time scales. Clim Dyn 25-5:461–476

Giorgi F, Mearns LO (1991) Approaches to the simulation of regional climate change: a review. Rev Geophys 29-2:191–216
Gutiérrez JM, Cofino AS, Cano R, Rodriguez MA (2004) Clustering methods for statistical downscaling in short-range weather forecast. Mon Wea Rev 132-9:2169–2183
Hennessey JP (1977) Some aspects of wind power statistics. J Appl Meteoro 16-2:19–128
Jiang Q, Smith RB, Doyle J (2003) The nature of mistral: observations and modeling of two MAP events. Q J R Meteorol Soc 129:857–875. doi:10.1256/qj.02.21
Kaas E, Li TS, Schmith T (1996) Statistical hindcast of wind climatology in the North Atlantic and northwestern European region. Clim Res 7:97–110. doi:10.3354/cr007097
Kaihatu JM, Handler RA, Marmorino GO, Shay LK (1998) Empirical orthogonal function analysis of ocean surface currents using complex and real-vector methods. J Atmos Ocean Technol 15:927–941. doi:10.1175/1520-0426(1998)015≤0927:EOFAOO≥2.0.CO;2
Levine E, Domany E (2001) Resampling method for unsupervised estimation of cluster validity. Neural Comput 13-11:2573–2593
Ludwig FL, Horel J, Whiteman CD (2004) Using EOF analysis to identify important surface wind patterns in mountain valleys. J Appl Meteorol 43:969–983. doi:10.1175/1520-0450(2004)043≤0969:UEATII≥2.0.CO;2
Michelangeli PA, Vautard R, Legras B (1995) Weather regimes: recurrence and quasi stationarity. J Atmos Sci 52-8:1237–1256
Millot C (1999) Circulation in the Western Mediterranean Sea. J Mar Syst 20:423–442. doi:10.1016/S0924-7963(98)00078-5
Moisselin JM, Schneider M, Canellas C, Mestre O (2002) Changements climatiques en France au 20ème siècle. Etude des longues séries de données homogénéises françaises de précipitations et températures. Meteorologie 38:45–46
Plaut G, Schuepbach E, Doctor M (2001) Heavy precipitation events over a few Alpine sub-regions and the links with large-scale circulation, 1971–1995. Clim Res 17:285–302. doi:10.3354/cr017285
Plaut G, Simonnet E (2001) Large-scale circulation classification, weather regimes, and local climate over France, the Alps and western Europe. Clim Res 17:303–324. doi:10.3354/cr017303
Pryor SC, Schoof JT, Barthelmie RJ (2005) Climate change impacts on wind speeds and wind energy density in northern Europe: empirical downscaling of multiple AOGCMs. Clim Res 29:183–198. doi:10.3354/cr029183
Pryor SC, Schoof JT, Barthelmie RJ (2006) Winds of change?: projections of near-surface winds under climate change scenarios. Geophys Res Lett 33:L11702. doi:10.1029/2006GL026000
Sailor DJ, Hu T, Li X, Rosen JN (2000) A neural network approach to local downscaling of GCM output for assessing wind power implications of climate change. Renew Energy 19:359–378. doi:10.1016/S0960-1481(99)00056-7
Siegismund F, Schrum C (2001) Decadal changes in the wind forcing over the North Sea. Clim Res 18:39–45. doi:10.3354/cr018039
Simmonds I, Keay K (2002) Surface fluxes of momentum and mechanical energy over the North Pacific and North Atlantic Oceans. Meteorol Atmos Phys 80:1–18. doi:10.1007/s007030200009
Stephenson DB, Hannachi A, O'Neill A (2004) On the existence of multiple climate regimes. Q J R Meteorol Soc 130:583–605. doi:10.1256/qj.02.146
Stephenson DB, Pavan V, Collins M, Junge MM, Quadrelli R (2006) Participating CMIP2 modeling groups. North Atlantic oscillation response to transient greenhouse gas forcing and the impact on European winter climate: a CMIP2 multi-model assessment. Clim Dyn 27:401–420. doi: 10.1007/s00382-006-0140-x
Stone DA, Weaver AJ, Stouffer RJ (2001) Projection of climate change onto modes of atmospheric variability. J Clim 14:3551–3565. doi:10.1175/1520-0442(2001)014≤3551:POCCOM≥2.0.CO;2
Straus DM, Molteni F (2004) Circulation regimes and SST forcings: results from large GCM ensembles. J Clim 17-8:1641–1656. doi:10.1175/1520-0442(2004)017≤1641:CRASFR≥2.0.CO;2
Taylor KE (2001) Summarizing multiple aspects of model performance in single diagram. J Geophys Res 106:D7. doi:10.1029/2000JA002008
Terray L, Demory ME, Déqué M, Coetlogon G, Maisonnave E (2004) Simulation of late-twenty first century changes in wintertime atmospheric circulation over Europe due to anthropogenic causes. J Clim 17-24:4630–4635
Troen I, Petersen EL (1989) European wind atlas. Risø national laboratory, Roskilde. ISBN 87-550-1482-8
Uppala SM, Kallberg PW, Simmons AJ, Andrae U, a Bechtold V, Fiorino M et al (2005) The ERA-40 re-analysis. Q J R Meteorol Soc 131:2961–3012. doi:10.1256/qj.04.176
Vautard R (1990) Multiple weather regimes over the North Atlantic: analysis of precursors and successors. Mon Weather Rev 118:2056–2081. doi:10.1175/1520-0493(1990)118≤2056:MWROTN≥2.0.CO;2
von Storch H (1995) Inconsistencies at the interface of climate impact studies and global climate research. Meteorol Z NF 4:72–80
von Storch H (1999) On the use of 'inflation' in statistical downscaling. J Clim 12:3505–3506. doi:10.1175/1520-0442(1999)012≤3505:OTUOII≥2.0.CO;2
Wilby RL, Charles SP, Zorita E, Timbal B, Whetton P, Mearns LO (2004) Guidelines for use of climate scenarios developed from statistical downscaling methods. Data distribution center of the intergovernmental panel on climate change
Wolf J, Woolf DK (2006) Waves and climate change in the north-east Atlantic. Geophys Res Lett 33:L06604. doi:10.1029/2005GL025113
Zorita E, von Storch H (1999) The analog method as a simple statistical downscaling technique: comparison with more complicated methods. J Clim 12:2474–2489. doi:10.1175/1520-0442(1999)012≤2474:TAMAAS≥2.0.CO;2